Progress in Oceanography 204 (2022) 102795

Contents lists available at ScienceDirect

Progress in Oceanography

journal homepage: www.elsevier.com/locate/pocean

Seasonal circulation and volume transport of the Bransfield Current

Marta Veny *, Borja Aguiar-González, Ángeles Marrero-Díaz, Ángel Rodríguez-Santana

Departamento de Física, Universidad de Las Palmas de Gran Canaria, Campus Universitario de Tafira, 35017 Las Palmas, Spain

ARTICLE INFO

Keywords:
Bransfield Current
South Shetland Islands
Direct Velocity Measurements
Dynamic structure
Volume transport
Seasonal and spatial variability

ABSTRACT

We present the first observational-based assessment of the seasonal circulation and volume transport driven by the Bransfield Current (BC), a surface-intensified coastal jet which flows northeastward along the southern slope of the South Shetland Islands (SSI) in the Bransfield Strait (BS). To this aim, we construct a seasonal climatology based on an extensive dataset of direct velocity measurements which were routinely collected along ship tracks from 375 cruises between 1999 and 2014. A major finding is that the BC is a year-round feature of the circulation in the BS, flowing persistently towards the northeast along the southern slope of the SSI. Along its full path, core velocities of the BC deepen down to at least 200–250 m depth. Maximum velocities are found to reach 60 cm s^{-1} during summer, and 40 cm s^{-1} during autumn and spring. Available measurements confirm the BC also flows northeastward during wintertime, at least from Nelson Island to King George Island, with maximum core velocities about 40 cm s^{-1}. The spatial variability along the SSI shelf suggests two distinct regions for the BC: a narrower jet of ~20–30 km upstream of Nelson Strait, and a wider jet of ~40 km downstream. Upstream of Nelson Strait, the BC transports about 0.93 ± 0.15 Sv in summer, 0.88 ± 0.19 Sv in autumn and 0.65 ± 0.13 Sv in spring. Available observations during winter lead to weaker transports about 0.50 ± 0.04 Sv from Greenwich Island to Nelson Strait. Downstream of Nelson Strait, volume transport estimates show no significant differences among seasons being on average 1.31 ± 0.20 Sv. As compared to upstream of Nelson Strait, the year-round average volume transport is weaker and about 0.74 ± 0.13 Sv. A mass balance analysis supports that this downstream increase in volume transport is likely due to a recurrent inflow passing through Nelson Strait and feeding the BC with source waters coming from the northern slope of the SSI. These results highlight that future observational efforts must focus on assessing the seasonal hydrography of the BC with mesoscale-solving measurements, especially when noting that the BC has been shown in the past to behave as a summertime buoyancy-driven coastal jet driving relatively warm and fresh Transitional Zonal Water with Bellingshausen influence (TBW), whose presence in the BS might be limited during winter.

1. Introduction

The Bransfield Strait (BS) is a semi enclosed region located between the Antarctic Peninsula (AP) and the South Shetland Islands (SSI). Based on summertime data, previous studies have described the circulation in BS as consisting of western and eastern inflows circulating cyclonically (Grelowski et al., 1986; Hofmann et al., 1996; Zhou et al., 2006; Sangrà et al., 2017) with a street of mesoscale anticyclonic eddies (AEs) of Transitional Zonal Water with Bellingshausen influence (TBW) characteristics in between (Sangrà et al., 2011, 2017). A sketch of this summertime circulation and major water masses is presented in Fig. 1a. The schematics of the vertical structure of the Bransfield Current System are presented in Fig. 1b.

The western inflow, namely the Bransfield Current (BC; Niller et al., 1991; Zhou et al., 2002, 2006), travels northeastward along the southern slope of the SSI as a coastal jet transporting TBW ($\theta > -0.4$ °C and salinity < 34.45 at 0–300 m depth). TBW is a well-stratified and relatively warm and fresh water, seasonally originated in the Bellingshausen Sea and Gerlache Strait due to summer heating and ice melting (Tokarczyk, 1987; García et al., 1994; Sangrà et al., 2011). At deeper levels (>300 m), a continuous tongue of cooled Circumpolar Deep Water (CDW) of about $-0.4 < \theta < 0.8$ °C and $34.4 < S < 34.5$ (Sangrà et al., 2017) flows also hugging the southern SSI slope underlying the BC.

The eastern inflow in BS, the Antarctic Coastal Current (CC), travels southwestward transporting Transitional Zonal Water with Weddell Sea influence, TWW, ($\theta < -0.4$ °C and salinity > 34.45), countering the northern Antarctic Peninsula coastline and spreading through the interior of the Strait. TWW is distinguished by colder and saltier waters than

* Corresponding author at: Edificio de Ciencias Básicas, Campus Universitario de Tafira, 35017 Las Palmas, Spain.
E-mail address: marta.veny@ulpgc.es (M. Veny).

https://doi.org/10.1016/j.pocean.2022.102795
Received 24 August 2021; Received in revised form 16 February 2022; Accepted 7 April 2022
Available online 15 April 2022

TBW, coming from the Weddell Sea (Tokarczyk, 1987; García et al., 1994) and being rather homogeneous throughout the water column (Grelowski et al., 1986; Hofmann et al., 1996; García et al., 2002; Zhou et al., 2002).

At surface and about 20–30 km from the peninsula slope, TBW encounters TWW forming the Peninsula Front, PF (García et al., 1994; López et al., 1999), a mesoscale shallow structure of 10 km wide, extending from the surface down to 100 m (Sangrà et al., 2011). At depth, TWW widens its domain over the whole Strait and encounters TBW being transported by the BC near the southern SSI slope, where they form the subsurface Bransfield Front (BF) between 50 and 400 m (Niller et al., 1991; García et al., 1994; López et al., 1999). Generally, the BF extends from 10 to 20 km, and is wider and shallower at the beginning of the BC pathway (Sangrà et al., 2011).

Initially, both Niller et al. (1991) and Zhou et al. (2002, 2006) described the BC as a western boundary current driven in the interior of the strait by a negative wind stress curl and the β-effect. However, following *in situ* hydrographic observations and laboratory experiments, Sangrà et al. (2011, 2017) and Poulin et al. (2014) showed that the BC propagates more consistently as a buoyant gravity current; the buoyant less-dense TBW flows along the SSI slope over the denser TWW, constrained in a narrow coastal band by the Coriolis force and by the buoyancy-induced pressure gradient. The width of the BC is typically 20 km, where central jet velocities reach 40–50 cm s^{-1} near the surface (Zhou et al., 2002, 2006), decaying linearly towards the bottom (Morozov, 2007; Savidge and Amft, 2009, Poulin et al., 2014).

Based on summertime hydrographic data, Sangrà et al. (2017) completed the description of the Bransfield Current System with the identification of TBW also north of the SSI, suggestive of the recirculation pathway of the BC around the SSI, as also supported by surface drifter trajectories and laboratory experiments (Fig. 1a).

Given the above scenario, accounting for a proper description of the seasonal variability, modulating the circulation in BS is relevant for achieving a better understanding of the warm/cold water pathways defining the oceanic forcing to glacier retreat in this basin (Cook et al., 2016). However, only a handful of summertime studies investigate the full path of the BC flowing along the SSI slope.

Based on geostrophic estimates (0–500 db), the summertime volume transport of the BC has been reported to range between 0.38 Sv and 0.88 Sv along the southern SSI slope (Sangrà et al., 2011, 2017). After arrival to the northeastern tip of King George Island, and recirculation around the archipelago, the south-westward volume transport driven by the BC along the northern shelf of the SSI decreases to 0.10–0.19 Sv (Sangrà et al., 2017).

Notably, few works have presented and analysed the BC vertical structure based on direct velocity measurements (Morozov, 2007; Savidge and Amft, 2009; Poulin et al. 2014). Up to date, the most comprehensive description of the circulation and transport in the Bransfield Strait was developed based on an extensive dataset of direct velocity measurements routinely collected along ship tracks performed by R/V Nathaniel B. Palmer and R/V Laurence M. Gould between 1997 and 2003 (Savidge and Amft, 2009). This study provided the first description of the summer velocity field and transport along the full pathway of the BC south of the SSI, finding that the jet deepens, and transport increases downstream south of Livingston Island. Velocities in the jet were reported to reach 50 cm s^{-1}, exceeding 35 cm s^{-1} in the averaged layer between 40 and 200 m depth. The increase in volume transport was estimated as 1 Sv in the vicinity of Boyd Strait to 2 Sv east of Livingston Island (Savidge and Amft, 2009). With regards to winter, these authors report a flow through Boyd Strait turning eastward into the Bransfield Strait and feeding directly into the BC (Savidge and Amft, 2009); however, downstream of Deception Island their data collection lack measurements to confirm the BC also drives a strong eastward jet along the southern shelf of the SSI (see Figure 10 in Savidge and Amft, 2009). Thus, the record long means from the binned shipboard ADCP velocities between 40 and 200 m depth (their Fig. 6) is constructed from, most of the BC extent, on summertime data. This prevents the confirmation of a strong eastward jet present in all seasons, especially when spring and autumn fields are omitted in their summer-winter view of the circulation.

In this work we use the same dataset of direct velocity measurements as in Savidge and Amft (2009), but here extended to a total of 375 cruises performed between 1999 and 2014. This data extension (about ten more years of observations) allows us to update the view presented in Savidge and Amft (2009), providing the first description of the velocity field and volume transport driven by the BC through all seasons

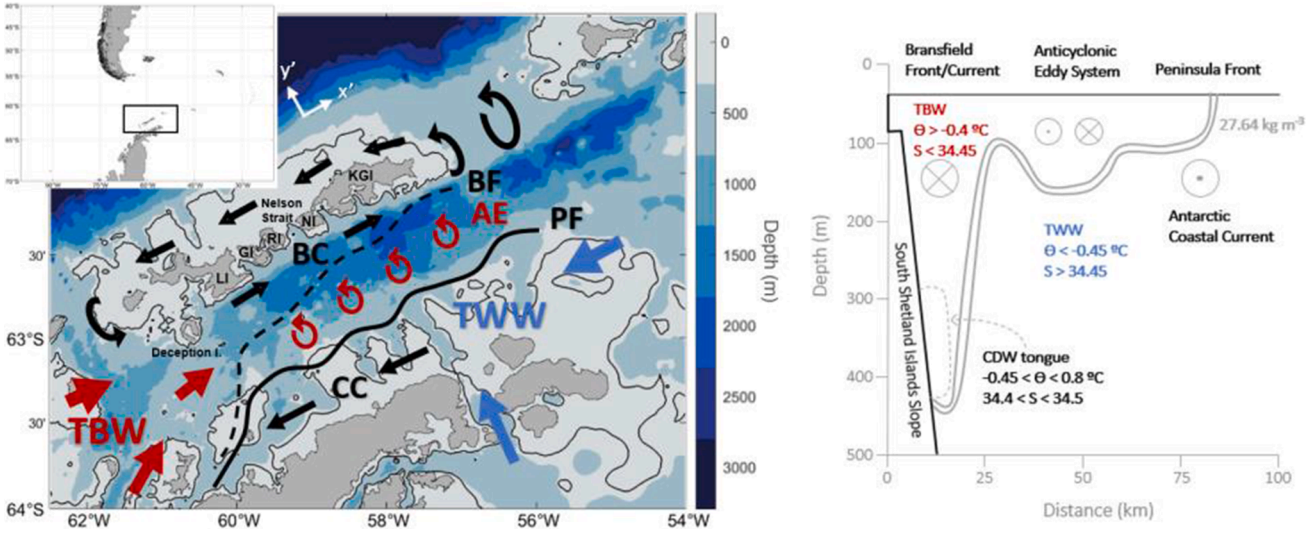

Fig. 1. (a) Bathymetric map of the Bransfield Strait and summertime circulation pattern of the Bransfield Current System as described in Sangrà et al. (2011, 2017). Acronyms for SSI are LI (Livingston Island), GI (Greenwich Island), RI (Robert Island), NI (Nelson Island) and KGI (King George Island). The plotted axes indicate the rotation of the coordinate system in along-slope, *x'*, and cross-slope, *y'*, directions. The isobath of 200 m is highlighted with a black contour. Acronyms for major features follow: AE (Anticyclonic Eddy), BC (Bransfield Current), BF (Bransfield Front), CC (Antarctic Coastal Current), PF (Peninsula Front), TBW (Transitional Bellingshausen Water), TWW (Transitional Weddell Water). (b) Sketch of the main components of the Bransfield Current System along a vertical section crossing the strait (modified from Figure 14 in Sangrà et al. (2011)) and the location of TBW (red) and TWW (blue). The Circumpolar Deep Water (CDW, black) tongue is distinguished by its temperature which is relatively higher than the surrounding waters. The spatial scales and ocean property ranges of each feature are indicated.

and over nearly its entire pathway of circulation south of the SSI. The paper is organized as follows. In Section 2, we describe data and methods. In Section 3, we present the results. First, we focus on the seasonal and spatial variability of the horizontal and vertical structure of the BC velocity field (Sections 3.1 and 3.2, respectively). Second, we estimate the seasonal volume transport driven by the BC along the southern slope of the SSI (Section 3.3). Last, we perform a mass balance analysis to elucidate the origin of the year-round increase in volume transport occurring east off Nelson Strait (Section 3.4). In Section 4, we discuss the observed variability of the BC against the literature. Section 5 closes the paper with a summary of the main conclusions.

2. Data and methods

We use an updated version of the data collection analysed in Savidge and Amft (2009), which extends the initial period 1997–2003 towards 2014. The data collection originates from two extensive datasets of direct velocity measurements collected with 150 kHz 'narrow band' Shipboard Acoustic Doppler Current Profilers (SADCPs) along ship tracks from R/V Nathaniel B. Palmer and R/V Laurence M. Gould, which navigated routinely from South America to Antarctica for logistical operations during all the seasons. Data acquisition and initial processing were accomplished by Dr. Eric Firing (University of Hawaii) and Dr. Teresa Chereskin (Scripps Institution of Oceanography). Velocity profiles were acquired and processed with UHDAS (University of Hawaii Data Acquisition System) and CODAS (Common Ocean Data Access System), respectively. The processed 5 min averaged transect data we use in this work can be found at the Joint Archive for Shipboard ADCP (JASADCP) webpage, http://ilikai.soest.hawaii.edu/sadcp/index.html. For additional processing details the reader is referred to Lenn et al. (2007) and Firing et al. (2012).

Initially, in the updated data collection we analyse, R/V Nathaniel B. Palmer contributes with 820,146 profiles from 100 cruises, performed between 1999 and 2013; and R/V Laurence M. Gould contributes with 130,280 profiles from 275 cruises, performed between 1999 and 2014. Profiles collected from R/V Nathaniel B. Palmer have a vertical resolution of 8 m from 31 to 503 m depth, while profiles collected from R/V Laurence M. Gould have a vertical resolution of 10 m from 30 to 1040 m depth. We address vertical interpolation on standard depth levels through both datasets towards a common 10 m vertical resolution starting at 30 m depth. Additionally, all individual data points outside a two-standard-deviation threshold were removed (Fischer and Visbeck, 1993) and replaced by linear interpolation.

Before gridding the data, as will be detailed in the following section, the barotropic tidal signal was removed using the Circum-Antarctic Tidal Simulation (CATS2008), an update to the model described by Padman et al. (2002). The derived model predictions for each measurement, at a given location and time, were taken as the best estimate of tidal magnitude and phase to remove from the data. Using a previous version of this same model, Savidge and Amft (2009) reported that predicted tidal velocities of mixed nature (diurnal and semidiurnal tides) were present at the shelf-edge and near the SSI in the Bransfield Strait. Thus, the four major tidal constituents (diurnal and semidiurnal) were accounted for the removal of the tidal signal in this work. However, we observe that the resulting fields turn out to be rather insensitive to the removal of the tidal signal (as it occurred in Savidge and Amft (2009)), given that mean and seasonal circulation features appear similarly using either detided or undetided data.

Finally, we must note that the nature of the present observations, obtained in an opportunistic manner (ship tracks from logistic operations), introduce some data limitations in the form of irregular samplings in space and time. Hence, in the following subsections, we address the gridding procedure, data density analyses, and error analyses such that we account for the impact of these data limitations when discussing later our results.

2.1. Climatology of the seasonal circulation

The procedure followed to construct the climatology we used to analyse the variability of the seasonal velocity field is described in this section. Seasons are defined following Zhang et al. (2011) and Dotto et al. (2021), as: summer (January-February-March), autumn (April-May-June), winter (July-August-September) and spring (October-November-December).

To account for the irregular nature of the data distribution, which is not uniform in space, we need to select the largest possible size still capturing mesoscale structures so we can retain the highest velocity profile population per each grid cell. To this aim, we select as cell size the Rossby radius of deformation, which is on the order of 10 km (Chelton et al., 1998). The resulting grid domain is shown in Fig. 2.

Because the data distribution is also irregular in time, we apply the step-by-step time-averaging scheme in Fig. 3 where for every grid cell, and at all depth levels, velocity profiles are averaged at increasing timescales. Then, velocity profiles are first averaged when sampling the same month and year. Second, the resulting monthly velocity profiles are averaged when sampling the same season and year. Finally, the seasonal profiles of every year are averaged per grid cell into climatological seasonal profiles. Thus, the number within each grid cell in Fig. 2 indicates how many seasonal profiles exist at a given location (i. e., a number of 5 indicates that there are 5 velocity profiles of a given season from 5 different years).

Through the time-averaging scheme, and given that some months and years are undersampled, we take a key assumption: ocean dynamics occurring through a given season evolve similarly through every month of that given season for any year. This assumption attempts to account for the fact that certain months and years are absent at some locations. We make the reader aware of this through the data density maps in Fig. 2 not to observe our end results as the product of equally weighted averages at all locations (a situation otherwise unachievable when counting with an irregular sampling).

Importantly, through the time-averaging scheme, we apply a vertical minimum coverage criterium of 90% of data availability between 30 and 250 m depth (the vertical range of study, as explained in the following section). We do this to prevent the rise of artificial staircases, which could appear as an artifact of averaging profiles with different vertical ranges of depth.

Based on these data density distributions, we select as the focus of our study the cells highlighted in black in Fig. 2, which capture the pathway of the BC at its best spatial coverage possible. Then, we use the seasonal velocity profiles over this domain to construct maps of the horizontal velocity field. To this aim, we apply the 2D interpolation tool developed by D'Errico (2022). Based on sparse linear algebra and PDE discretizations, this tool attains consistency with the original data field.

Error estimates are computed considering the instrument error of the SADCP measurements, which is 0.5 cm s^{-1} (Instruments, 2013), plus the Standard Error of the Mean (SEM, as computed in Savidge and Amft (2009)) accounting for all the profiles falling within a given grid cell and time-step of the averaging procedure in Fig. 3. In the few cases where the SEM cannot be computed due to the solely existence of one velocity profile falling within a given grid cell and time-step, the associated errors account only for the instrument error.

2.2. Along/cross-slope rotation and volume transport

In order to assess properly the structure of the Bransfield Current according to its propagation parallel to the southern slope of SSI, we rotate counterclockwise the cartesian coordinate system along-slope (x') and cross-slope (y'). The rotation angle is 36.25°, which responds to the mean angle of all the cross-slope grid cells highlighted in black in Fig. 2. In each cell grid, the east and north components of seasonal velocity profiles are rotated, obtaining along-slope (u') and cross-slope (v') seasonal velocity components.

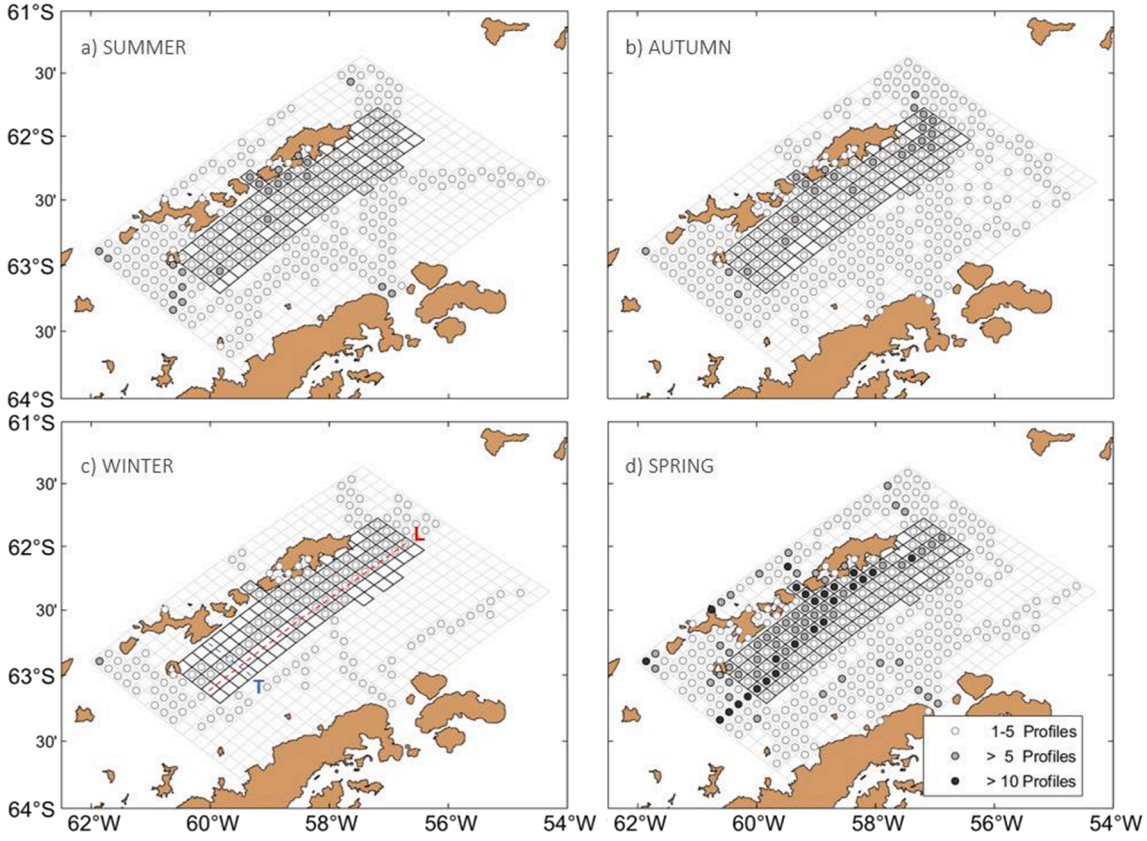

Fig. 2. Maps of seasonal data density showing the amount of climatological seasonal velocity profiles per year obtained for each grid cell of 10x10 km in the area of study, from 1999 to 2014 (see legend). Panels follow seasons as: a) summer, b) autumn, c) winter, and d) spring. The grid cells highlighted in black indicate the domain used to construct along-slope (L) and cross-slope (T) transects (see panel c) for the study of the variability of the BC.

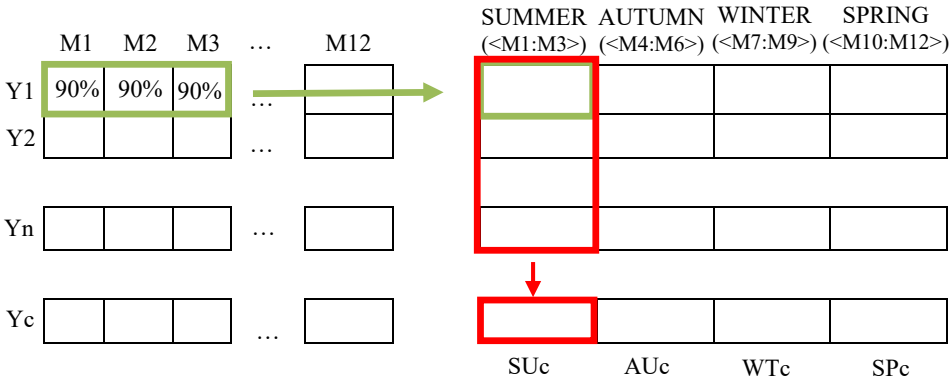

Fig. 3. Time-averaging scheme for the generation of the climatological velocity profiles falling within each grid spatial cell showed in Fig. 2. The time-averaging codes are defined as follows: M#, is the monthly averaged velocity of the month #; Y#, is the yearly averaged velocity of the year #; SUc, AUc, WTc and SPc, are the seasonal climatological averages. The computation of the climatological velocity profiles per grid cell includes only those profiles of which have measurements in, at least, a 90% of the first 250 m of the profile to prevent artificial stepwise structures.

The along-slope (U') and cross-slope (V') seasonal volume transport estimates are computed following:

$$U'(x',t) = \int_0^{D_T} \int_{-h}^{-h_0} u' dz dy', \quad (1)$$

$$V'(y',t) = \int_0^{D_L} \int_{-h}^{-h_0} v' dz dx', \quad (2)$$

where x' is the along-slope coordinate; y' is the cross-slope coordinate; u' (m s^{-1}) and v' (m s^{-1}) are along-slope and cross-slope seasonal velocity components, respectively; D_T (m) and D_L (m) are the lengths of the cross-slope and along-slope transects, denoted as T_i (i = 1, 21) and L_j (j = 1,4) transects, respectively; h_0 (m) is the depth of the shallowest available velocity; and, h (m) is the depth of the deepest available velocity.

In all cases, h_0 and h are 30 m and 250 m, respectively. The value of h = 250 m for the computation of volume transport estimates follows reasonably from previous works where the Bransfield Current was shown to propagate as a coastal flow with a layer thickness about 200–300 m (Morozov, 2007; Savidge and Amft, 2009; Sangrà et al., 2011, 2017).

The cross-slope transects generally depart from the slope south off the SSI and span towards the middle of Bransfield Strait all along the SSI. Thus, D_T is generally 30 km, except when the grid cell most coastward/oceanward is absent; then, D_T becomes 10 km shorter. Upon data availability, the along-slope transects we use in this study are constrained to the domain spanning from Nelson Strait to midst of King George Island (T10-T14) and, thus, D_L is 40 km in all cases.

Prior to calculation of volume transport estimates following Eqs. (1) and (2), we apply a similar interpolation work to that accounted for in the previous section for the construction of the horizontal maps of the velocity field. Thus, we use the 2D interpolation tool developed by D'Errico (2022) through all T and L transects over data gaps equal/shorter than 20 km between grid cells. By data gap, we mean here either the absence of a vertical profile within a given grid cell or the presence of a vertical profile which is shorter than spanning from 30 to 250 m depth. Through this interpolation procedure, we achieve transects which have a common vertical spatial coverage. This enables a robust comparison among volume transport estimates, avoiding under/over estimations when data gaps existed prior to interpolation. Exceptions occur on a few cases where one of the four grid cells at the T transects is missing and still an associated volume transport estimate is provided. These cases will be noted in the text through our discussion of the results to prevent the reader about straightforward comparisons.

Anywhere in the text where a ± quantity is indicated next to volume transport estimates, that amount refers to the propagated error from sum of the instrument error and the SEM associated to each seasonal velocity profile composing the transect.

3. Results

Through this section we characterize the horizontal and vertical structure of the Bransfield Current using climatological fields constructed from direct velocity measurements (Section 3.1 and Section 3.2, respectively). We also estimate the volume transport driven by the upper 250 m of the Bransfield Current, varying seasonally and spatially along its pathway south of the South Shetland Islands (Section 3.3). Finally, in Section 3.4, we perform a mass balance analysis east off the Nelson Strait to elucidate the origin of the observed volume transport increase of the BC.

3.1. Seasonal variability of the Bransfield Current: horizontal structure

The seasonal climatology of the horizontal circulation driven by the BC is presented in Figs. 4 and 5 following depth-averaged velocities within the 80–100 m and 130–150 m layers, respectively (velocity vectors smaller than associated errors are not shown). These two depth ranges are selected to account for the decrease in strength of the BC at depth, as previously found in summertime and springtime observations (Morozov, 2007; Savidge and Amft, 2009; Sangrà et al., 2011, 2017).

The most outstanding feature is the recurrence of a northeastward-flowing coastal jet circulating parallel to the southern slope of the South Shetland Islands, from Livingston Island to King George Island along a path of 170 km in all seasons but in winter, when the current is also visible but over a shorter domain of available measurements spanning from Nelson Island to King George Island, a path of 90 km. Noting the similarity of this current to that one described in previous works for this region during summertime (e.g., Niller et al., 1991; Zhou et al., 2002, 2006; Sangrà et al., 2011, 2017; Poulin et al., 2014), we attribute the signal of this year-round coastal jet to the Bransfield Current.

Spatially, the BC appears as a well-organized, and relatively strong, coastal current flowing towards the northeast downstream of Livingston Island (T3-T4). Upstream of this location, near Deception Island (T1-T2), the flow appears through all seasons, but spring, less intense and not yet organized as a northeastward-flowing current. This spatial pattern agrees well with previous works based on summertime observations (Fig. 1a), here extending its recurrence through other seasons. When approaching the northeasternmost tip of King George Island, the recirculation of the BC around the archipelago is suggested to occur also year-round, although more clearly during winter and spring (Figs. 4 and 5). This recirculation had been previously demonstrated to occur at least during summertime (Sangrà et al., 2017), thus extending here its

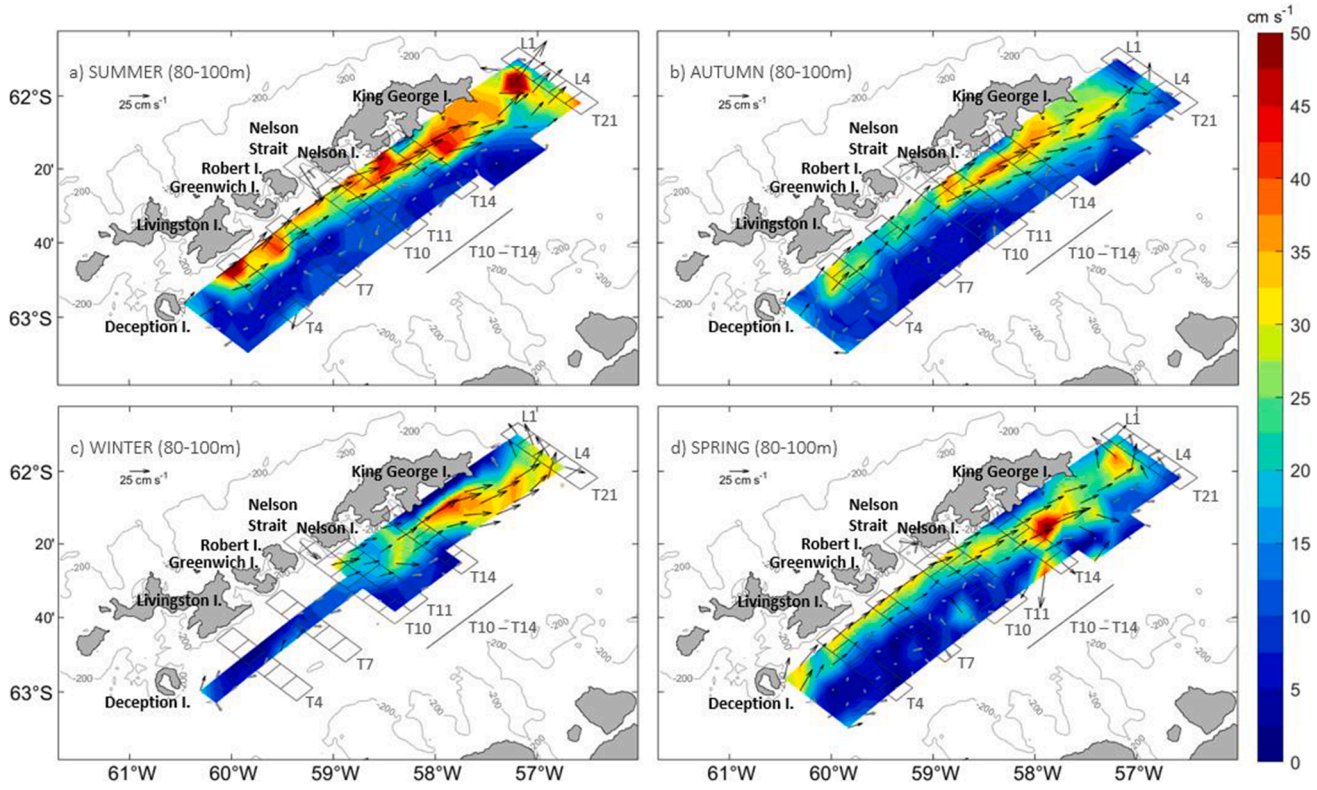

Fig. 4. Seasonal maps of the horizontal velocity field at 80–100 m following: a) summer, b) autumn, c) winter, and d) spring. Shades of colors are speed in units of cm s^{-1}. Scaled arrows represent direction and strength (only arrows with speed values above their associated error are shown and used for interpolation). Scaled arrows in black (gray) indicate magnitudes equal/above (below) 15 cm s^{-1}. Cross-slope (T_i) and along-slope (L_j) transects of study are also indicated in each panel. The T10-T14 line shows the area limited by these transects.

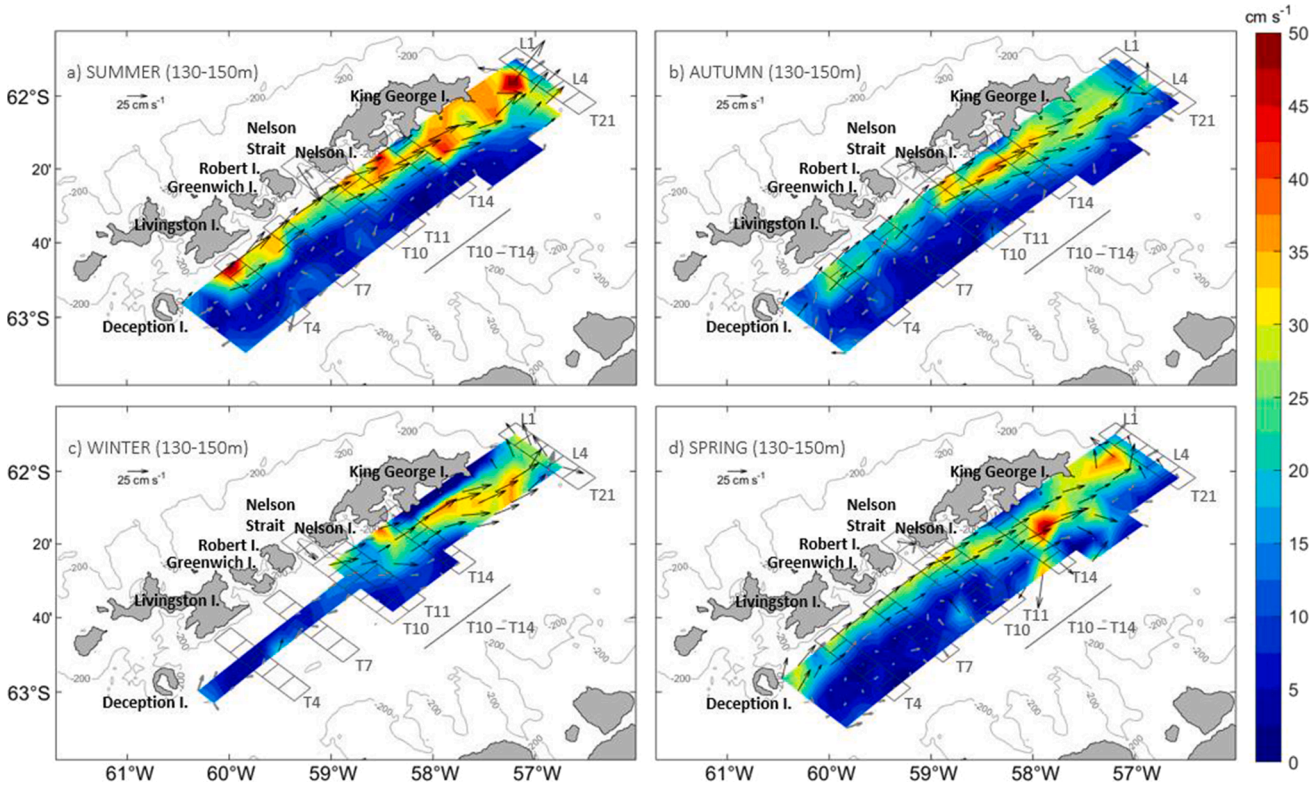

Fig. 5. Same as in Fig. 4 but for the depth range of 130–150 m.

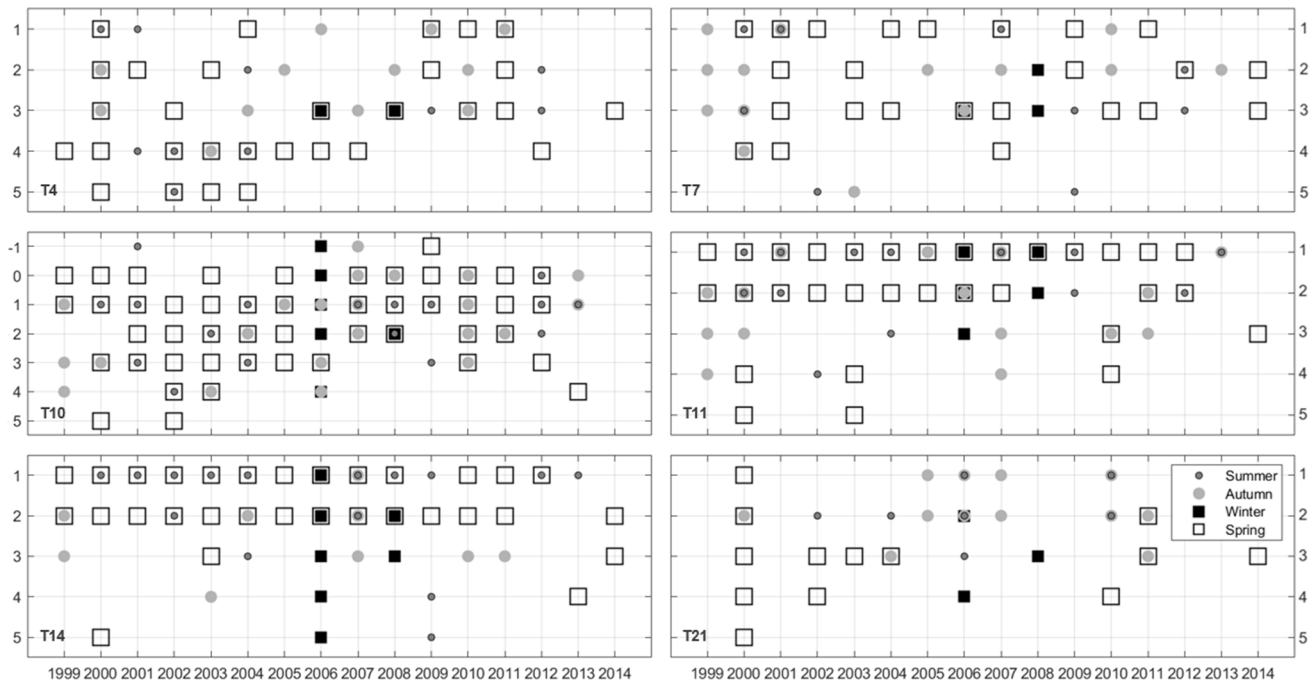

Fig. 6. Summary of the multiyear seasonal data used to construct the climatology shown in Fig. 7 for the along-slope transects T4, T7, T10, T11, T14 and T21 (see their location in Figs. 4 and 5). The values on the vertical axis are the values of the transects L. L-1 and L0 in T10 are those located in the Nelson Strait. A mark for a given grid cell over a specific year indicates that at least one profile exists for that season, so its size or shape is not proportional nor related to its value.

recurrence also through winter and spring.

Seasonally, results support that the BC flows at higher velocities during summer, reaching climatological values up to 60 cm s^{-1} and 50 cm s^{-1} at depths between 80-100 m and 130–150 m, respectively. The weakening of the BC at depth, as will be shown further in the following section for all seasons, is consistent with prior works based on direct velocity measurements: the springtime vertical transect presented in Morozov (2007); the summertime climatological vertical transects presented in Savidge and Amft (2009); and, the summertime velocity profiles presented in Poulin et al. (2014). During autumn, winter, and

spring the BC also flows as a relatively strong and continuous jet, peaking at about 40 cm s^{-1}.

Lastly, we note that a weaker flow exists seaward of the Bransfield Current in the peninsula cross-strait direction. This field near the middle of the strait, highly variable and not aligned to any prevailing direction, is consistent with the street of inter-frontal anticyclonic eddies reported in Sangrà et al. (2011, 2017).

3.2. Seasonal variability of the Bransfield Current: vertical structure

Through this section, we characterize the seasonal and spatial variability of the Bransfield Current in the upper 250 m of the water column based on vertical transects sourced with multiyear sampled grid cells. Noting that the horizontal velocity distributions in Figs. 4 and 5 show the circulation of the BC flows parallel to the southern slope of SSI, we investigate in the following the vertical structure of the BC after rotating its velocity components into *u'* and *v'*, where these represent the along-slope and cross-slope components, respectively (see section 2.2).

To characterize the along-slope structure of the BC we selected the cross-slope transects which were most repeatedly sampled over time, i.e. transects T4, T7, T10, T11, T14 and T21. A detailed summary of the multiyear seasonal data behind these transects is shown in Fig. 6. The distribution of available measurements covering different locations and seasons by years supports the coherence of the resulting climatological velocity fields presented in Fig. 7. In this latter figure, vertical sections of the T transects show only the along-slope component, *u'*, given that this captures the stream direction. The cross-slope component, *v'*, through the T transects (not shown) is generally negligible, as supported by the circulation patterns shown in Figs. 4 and 5.

A major finding is the confirmation of the BC as a strong and recurrent jet flowing northeastward along the slope of the SSI through all seasons ($u' > 0$ in red, Fig. 7) down to at least 250 m depth. In all vertical sections, the structure of the BC agrees well with the view of a surface-intensified coastal jet whose velocities decrease at depth, particularly from 100-150 m towards deeper levels (Fig. 7). This structure also agrees with the horizontal circulation pattern shown at different depths in Figs. 4 and 5.

Importantly, across all transects but transect T21, data density allows us to capture counterflows ($u' < 0$ in blue, Fig. 7) flowing towards the southwest, and likely attributable to the highly variable currents driven by the street of eddies sketched in Fig. 1, and visible in the horizontal velocity fields presented in Figs. 4 and 5. At T21, the vertical structure of the BC suggests the start of its recirculation around King George Island (Fig. 7), as also supported by Figs. 4 and 5.

Seasonally, the strengthening of the BC, as presented in the previous section, is also visible through its vertical structure (Fig. 7), flowing at higher maximum velocities during summertime at nearly all the transects (velocities up to 45 cm s^{-1}). The only exception occurs south of Nelson Island (transect T10), where the BC flows at 25 cm s^{-1} in summer and spring as opposed to higher velocities up to 35 cm s^{-1} in autumn and winter. The BC flows at an average speed of 25–35 cm s^{-1} during the other seasons across all the transects, except in transect T21, where velocities are generally lower (~10–20 cm s^{-1}).

Spatially, we find the BC displays a coherent pattern depending on whether it finds to its left-hand side the islands' slope or a channel between islands (Fig. 7). This is visible by comparison of transects T4, T7

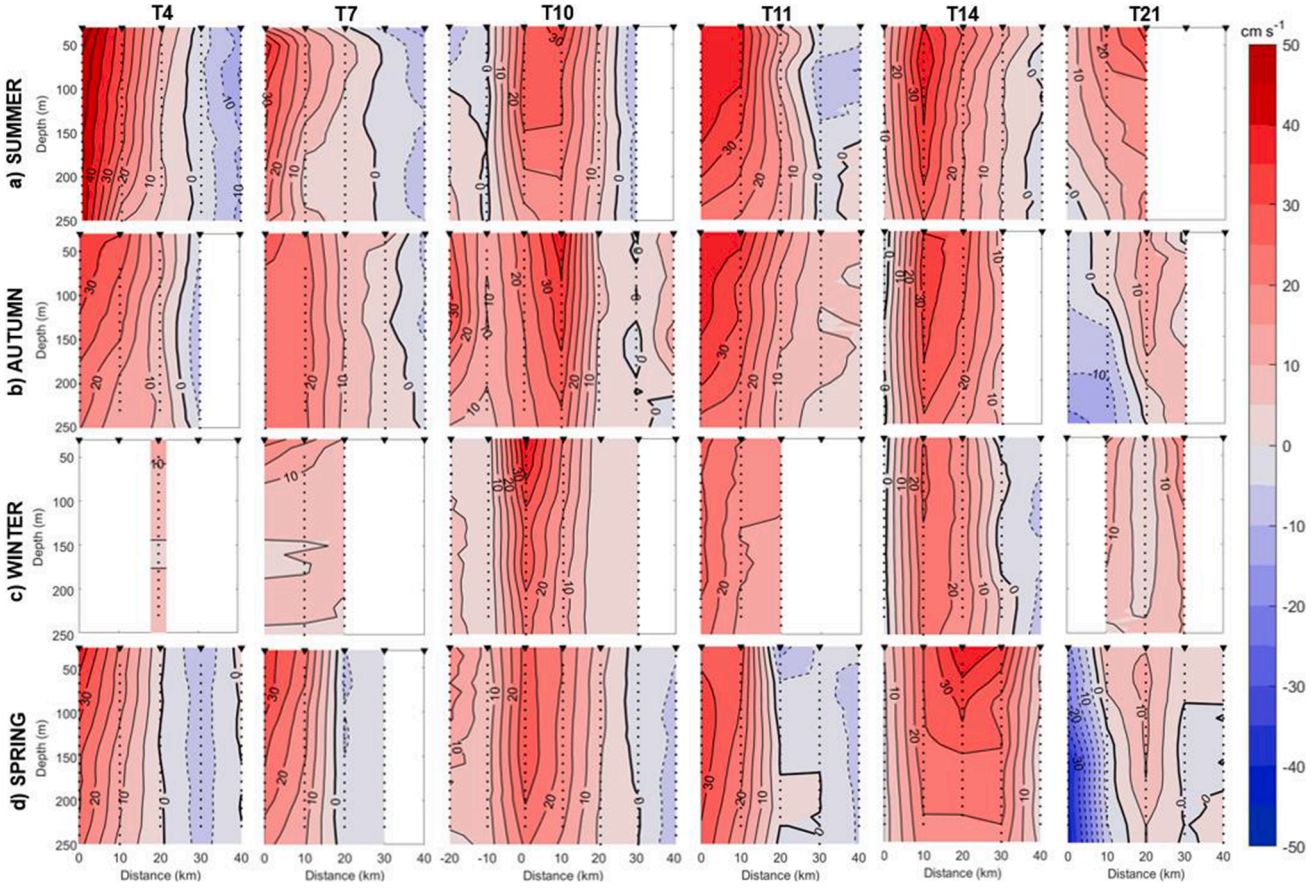

Fig. 7. Seasonal climatology of along-slope velocities measured by SADCPs in the upper 250 m of the water column at transects T4, T7, T10, T11, T14 and T21 (from left to right-hand side panels). Seasons follow (from top to bottom panels): a) summer, b) autumn, c) winter and d) spring. Distance starts at the southern SSI slope being perpendicular to the islands' slope (distance 0 km), except at transect T10, which departs from Nelson Strait at − 20 km. Velocity is positive (negative) towards the northeast (southwest) in the along-slope direction (see rotated coordinates *x'* and *y'* in Fig. 1a). The black dots along the vertical refer to original data points.

and T11, which show the BC south off the slope of Livingston Island, Greenwich Island and Nelson Island, respectively, against transects T10 and T14, which show the BC flowing south off channels between SSI. Along the former case (T4, T7 and T11), the BC appears hugging the islands' slope; along the latter case (T10 and T14), the BC appears flowing as a seaward wedge-shaped current.

Combining the horizontal structure of the BC (Figs. 4 and 5) along with its vertical structure (Fig. 7), one can observe how the northeastward-flowing jet (the BC) broadens from about 20–30 km wide upstream of Nelson Strait (T3-T9) towards about 40 km wide downstream of Nelson Strait (T11-T20). Upon data availability, we find this spatial pattern seems to be present year-round.

3.3. Seasonal variability of the Bransfield Current: along-shore volume transport

In this section we analyse the spatial and seasonal variability of the volume transport driven by the Bransfield Current along its full pathway south of the SSI. At this point, we recall that volume transport estimates follow from the 4 vertical profiles of horizontal velocity closer to the coast (where the BC and the highest data density are found), as described in Section 2.2 (Eqs. (1) and (2)).

Accordingly, Fig. 8 presents the seasonal estimates of the along-slope volume transport, U' (Sv), driven by the Bransfield Current through each transect of the study area. These transects are perpendicular to the island coastlines and to the stream direction of the Bransfield Current (see the grid cells accounting for each transect in Fig. 2). Importantly, we must note that only positive U' values (northeastward volume transport) have been taken into account when computing the volume transport driven by the Bransfield Current. This condition applies not to underestimate the transport of the BC when opposing flows are also acting across the transect. The errors obtained for each estimate of volume transport are indicated in Fig. 8. We find these errors vary from 0.02 to 0.62 Sv with an average value of 0.17 Sv.

Following the distinctive widths the BC exhibits upstream and downstream of Nelson Strait (see section 3.2), we analyse our estimates of volume transport according to these two zones. Upstream of Nelson Strait (T3-T9), we find the BC transports on average 0.93 ± 0.15 Sv in summer, 0.88 ± 0.19 Sv in autumn and 0.65 ± 0.13 Sv in spring. During wintertime, there is scarcity of data and transports from T7 to T9 account for an average of 0.50 ± 0.04 Sv. Downstream of Nelson Strait (T11-T20), we find the BC transports on average 1.53 ± 0.17 Sv in summer, 1.29 ± 0.26 Sv in autumn, 1.20 ± 0.15 Sv in winter and 1.22 ± 0.20 Sv in spring. These results suggest that upstream of Nelson Strait the BC transports the largest volumes of water through summer and autumn as compared to spring and winter, though accounting for the associated errors only winter stands out with a significatively weaker transport. Downstream of Nelson Strait, estimates of volume transport are generally higher than upstream and present no significative difference among seasons when accounting for their associated errors.

	Summer, U' (Sv)	Autumn, U' (Sv)	Winter, U' (Sv)	Spring, U' (Sv)	Mean, U' (Sv)
T1	0.57 ± 0.19	0.86 ± 0.21	0.24 ± 0.02*	0.77 ± 0.14	0.61 ± 0.14
T2	0.42 ± 0.03	0.43 ± 0.07	0.21 ± 0.02*	0.71 ± 0.34	0.44 ± 0.12
T3	0.90 ± 0.11	1.17 ± 0.13	-	0.54 ± 0.16	0.87 ± 0.13
T4	1.14 ± 0.28	0.93 ± 0.16	-	0.66 ± 0.10	0.91 ± 0.18
T5	0.70 ± 0.13	0.89 ± 0.21	-	0.54 ± 0.07	0.71 ± 0.14
T6	1.22 ± 0.21	0.63 ± 0.16*	-	0.82 ± 0.26	0.89 ± 0.21
T7	0.64 ± 0.11	0.98 ± 0.31	0.22 ± 0.03*	0.63 ± 0.11	0.62 ± 0.14
T8	0.85 ± 0.15	0.83 ± 0.19	0.42 ± 0.07*	0.71 ± 0.13	0.70 ± 0.13
T9	1.05 ± 0.09	0.72 ± 0.16	0.86 ± 0.03	0.65 ± 0.06	0.82 ± 0.09
T10	0.82 ± 0.25	1.34 ± 0.28	0.93 ± 0.12	1.12 ± 0.23	1.05 ± 0.22
T11	1.32 ± 0.18	1.36 ± 0.26	0.83 ± 0.13*	0.86 ± 0.13	1.09 ± 0.17
T12	1.41 ± 0.21	1.43 ± 0.24	1.02 ± 0.06	1.39 ± 0.13	1.31 ± 0.16
T13	1.71 ± 0.13	1.56 ± 0.22	1.69 ± 0.06	1.22 ± 0.47	1.55 ± 0.22
T14	1.31 ± 0.12	1.28 ± 0.15	0.92 ± 0.18	1.45 ± 0.12	1.24 ± 0.14
T15	1.40 ± 0.08	1.16 ± 0.30	0.99 ± 0.11*	-	1.18 ± 0.16
T16	1.47 ± 0.03	1.34 ± 0.36	1.60 ± 0.39	1.17 ± 0.16	1.40 ± 0.24
T17	1.42 ± 0.10	1.35 ± 0.48	1.38 ± 0.24*	1.37 ± 0.15	1.38 ± 0.24
T18	1.85 ± 0.06	1.50 ± 0.22	1.23 ± 0.08*	1.09 ± 0.23	1.42 ± 0.15
T19	-	-	-	-	-
T20	1.90 ± 0.62	0.62 ± 0.15	1.14 ± 0.14	-	1.22 ± 0.30
T21	0.59 ± 0.27*	0.26 ± 0.03	-	0.22 ± 0.05	0.36 ± 0.12

Fig. 8. Estimates of the northeastward along-slope volume transport (U' (Sv) > 0), and their associated error (Sv) for transects T1 to T21 based on SADCP measurements (the transects of study are shown in Figs. 4 and 5). The volume transport was computed from 30 m to 250 m depth, departing south of the SSI slope to 30 km offshore (L4). The error for each estimate is also indicated. The size of the coloured bars indicates the transport normalized against the largest value obtained for each season: summer (red), autumn (yellow), winter (blue) and spring (green). Estimates with an asterisk indicate transports computed across transects where D_T equals to 20 km instead of 30 km. See Section 2.2 and Eqs. (1) and (2) for further details.

In the following section we explore further the origin of the observed downstream increase in volume transport, which we attribute to the inflow of source waters feeding the BC through Nelson Strait, i. e. from the northern domain of the SSI to its southern domain.

From the transect T20 to T21, the BC volume transport decreases notably towards its nearly lowest values on record, suggestive of the current approaching its turning point for the recirculation around the SSI (the average transport estimate decreases from 1.22 ± 0.30 Sv to 0.36 ± 0.12 Sv).

3.4. Volume transport increase east of Nelson Strait

Through this section we perform a mass balance analysis following the box defined along-slope by the transects T10 and T14 and cross-slope by the transects L1 to L4 (see the location of the transects in Figs. 4 and 5). The aim is to elucidate whether the observed downstream increase in volume transport of the BC may be driven by an inflow through the Nelson Strait, i. e. in the direction through the transects L1 to L4. This inflow has been previously suggested to feed the BC with source waters coming from the northern shelf of the SSI based on hydrographic measurements (Gordo Rojas, 2013).

The mass balance analysis is presented in Fig. 9, where seasonal net transport estimates are indicated for each boundary of the box of study. Note that outgoing (incoming) transports are denoted as positive (negative) transports in red (blue) colors. For a better visualization of the transport signs, a scheme is added for the autumn study case.

In the following, we describe the results for summer as illustrative of the general pattern occurring through all seasons. Thus, in summer, we find the following inflows: an entry of 0.82 ± 0.25 Sv that flows through T10, driven by the BC, and an entry of 0.60 ± 0.18 Sv that flows through L1, driven by the currents through the Nelson Strait. Then, a small part of the latter contribution appears to recirculate towards the northeast (from L1 to L2-L4), while most of it joins the BC, exiting the box through the transect T14. As a result, we find an outflow of 1.31 ± 0.12 Sv exits the box, which accounting for the associated errors appear to be in approximate balance with the inflows. This structure is consistent with the horizontal velocity circulations observed in Figs. 4 and 5.

It is worthwhile noting that, generally, estimates for V' are lower than for U' since the former represents the cross-stream direction of the BC. However, seasonal estimates of V' confirm the recurrence over time of a southward current flowing through transects L1, L2 and L3, especially during summer and winter, when the flux coming from the Nelson Strait appears to be feeding the BC more prominently. When the flow reaches L4, the transport to the south appears lower as the influence of the Nelson Strait inflow diminishes.

4. Discussion

In this section, we focus on discussing the seasonal circulation and volume transport of the Bransfield Current as observed in our climatology, noting that uncovering the year-round driving forces of the current are beyond the scope of the present work.

4.1. Horizontal structure

Along its pathway south off the SSI, the Bransfield Current appears to follow the bathymetry orientation, as constrained to the coast by the Coriolis force through all the seasons (Figs. 4 and 5). When approaching the easternmost tip of King George Island, our climatologies suggest the BC starts its recirculation around the archipelago, as reported in previous works based on summertime observations (Sangrà et al., 2011, 2017). The start of the recirculation is mostly evident in Figs. 4 and 5 during winter and spring, thus our results suggest its recurrence also through other seasons. In this line, several studies have hypothesized that the transport of TBW around the SSI contributes to the fertilization of the waters along the northern shelf (Teira et al., 2012, García-Muñoz et al., 2014), which highlights the importance of further understanding the circulation around the islands. Furthermore, as a relatively warm water, the routes followed by TBW are key in a context of ocean forcing to glacier retreat around the SSI (Kreczmer et al., 2021), thus demanding a more comprehensive knowledge of the year-round hydrography contouring the SSI bathymetry.

		BOX		
		U' (Sv) T10	V' (Sv) L	U' (Sv) T14
Summer	L1	-0.82 ± 0.25	-0.60 ± 0.18	1.31 ± 0.12
	L2		-0.48 ± 0.17	
	L3		-0.08 ± 0.15	
	L4		-0.03 ± 0.08	
Autumn	L1	-1.34 ± 0.28	-0.37 ± 0.13	1.28 ± 0.15
	L2		-0.59 ± 0.22	
	L3		-0.35 ± 0.20	
	L4		0.07 ± 0.14	
Winter	L1	-0.93 ± 0.12	-0.60 ± 0.11	0.92 ± 0.18
	L2		-0.32 ± 0.14	
	L3		-0.51 ± 0.07	
	L4		-0.17 ± 0.05	
Spring	L1	-1.12 ± 0.23	-0.39 ± 0.17	1.45 ± 0.12
	L2		-0.38 ± 0.15	
	L3		-0.06 ± 0.24	
	L4		0.25 ± 0.29	

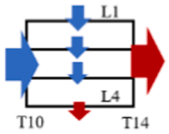

Fig. 9. Mass balance analysis showing the estimates of along-slope volume transports, U' (Sv), through the transects T10 and T14 (D_L = 40 km), and cross-slope volume transports, V' (Sv), through the transects L1 to L4. A positive (negative) value indicates outgoing (incoming) transports in red (blue) as shown in the scheme for the autumn study case. The error for each estimate is also indicated.

With regards to the speed magnitude, summertime averaged values of about 40 cm s^{-1} shown here for the velocity fields at 80–100 m and 130–150 m (Figs. 4 and 5, respectively) agree well the speed range of surface drifters deployed within the BC during the same season, and reporting average speeds also about 30–40 cm s^{-1} (Zhou et al., 2002; Sangrà et al., 2017). Although for a slightly different depth range of averages, these summertime jet velocities are also in good agreement with those reported across lines B and C in Savidge and Amft (2009), reaching 35 cm s^{-1} in the averaged layer between 40 and 200 m depth (line B, located south off Livingston; and, line C, located King George Islands). Available wintertime measurements in Figs. 4 and 5 not only confirm the BC flows at relatively strong speeds about 25 cm s^{-1} downstream of Nelson Island, but also that peak speeds can be found about 40 cm s^{-1} south off King George Island.

4.2. Vertical structure

The along-slope velocity field of the BC shows a coherent structure where the current flows persistently northeastward constrained to the islands' slope through all seasons (Fig. 7). However, we find some spatial variability regarding its dynamical core when comparing the structure displayed at cross-slope sections departing from the island's slope and when departing from the channel between islands (see the locations of cross-slope transects in Fig. 4). Thus, when south of the SSI, the core of the BC forms half of a wedge shape leaning on the island slope (transects T4, T7 and T11) while, between channels, a full wedge shape is visible due to the local detachment of the current from the island slope (transects T10, T14 and T21).

Seasonally, the vertical sections confirm that highest velocities through nearly its full pathway are found during summertime with near-surface core velocities up to 45–50 cm s^{-1} (Fig. 7). However, during the other seasons, the BC also flows as a relatively strong and continuous jet with core velocities up to 30–35 cm s^{-1} (Fig. 7).

Generally, the spatial variability of the BC displays two distinct regions: upstream and downstream of Nelson Strait (Figs. 4, 5 and 7). Through the first region (transects T3-T9), the BC exhibits from spring to autumn a horizontal width between 20 and 30 km. Downstream of Nelson Strait (transects T11-T20), the BC widens in all seasons another 10 km offshore, likely promoted by the widening of the King George Island shelf (see the isobath of 200 m in Figs. 4 and 5), which forces the current to lean over the slope further offshore.

Interestingly, the above pattern along the islands' southern shelf, distinguishing between a narrower region and a wider region, upstream and downstream of Nelson Strait, respectively, is also in agreement with previous studies describing the dynamical properties of density-driven coastal currents. Münchow and Garvine (1993) investigated this type of currents when analyzing the Delaware Coastal Current. In this study case, the outflow of buoyant waters from the Delaware Estuary drives lateral density gradients sustaining an alongshore current which remains trapped near the coast by the Coriolis force. The authors also described two dynamically distinct regions, which they termed as the source and plume regions. Through the source region, they find a current whose width scales well with the internal deformation radius. Farther downstream, in the plume region, the authors find much reduced lateral density gradients and a current much wider than the deformation radius. This is also the case for the BC when accounting for the internal deformation radius. An analogous pattern is also observed in laboratory experiments when reproducing the scales of the BC in a rotating tank (Sangrà et al., 2017). The authors show that the lab-simulated BC also widens downstream, before starting its recirculation around a wall mimicking the SSI archipelago (see Figure 11 in Sangrà et al. (2017)). Notably, the downstream widening of the jet in these two latter works appears without invoking the widening of the shelf. This suggests that both the internal dynamics of the density-driven coastal current and the shelf widening of King George Island may add to the downstream widening of the BC.

4.3. Volume transport

The volume transports (30–250 m) presented in Fig. 8 reveal several major features regarding spatial and temporal variability of the BC along its pathway and through seasons.

Upstream of the Nelson Strait, we find the BC presents similar volume transports in summer, autumn and springtime (0.93 ± 0.15 Sv, 0.88 ± 0.19 Sv and 0.65 ± 0.13 Sv, respectively). However, the transport appears to decrease notably during winter, as compared to other seasons, at least south off Greenwich Island to Nelson Strait (0.50 ± 0.04 Sv in transects T7-T9). We hypothesize that this seasonal variation may be driven by the different nature of the inflow feeding the BC during winter, when source waters of the BC might be potentially fed from sea-ice formation areas in the Bellingshausen Sea and Gerlache Strait. This different source waters would approach the water mass properties of TBW to those of the cooler and saltier TWW. The latter phenomenon would then account for a relaxation of the buoyancy-induced pressure gradient that has been shown to sustain the BC at least during summer in previous works (Sangrà et al., 2011, 2017).

Downstream of Nelson Strait, the seasonally-averaged estimates of volume transport suggest that no significant variability exists among seasons, presenting on the main significantly higher transports than estimates obtained farther upstream. This increase in volume transport occurring after passing the Nelson Strait is consistent with prior summertime data presented in Savidge and Amft (2009) and Sangrà et al. (2011), based on direct velocity measurements and geostrophic velocity estimates, respectively. The novelty is that our observations show this spatial pattern is also present through autumn, winter and spring based on direct velocity measurements. We hypothesize the downstream increase in volume transport may be driven by a recurrent inflow passing through Nelson Strait (Figs. 4 and 5) and feeding the BC with source waters coming from the northern slope of the SSI. The existence of this inflow feeding BC has been previously suggested by at least one previous work (Gordo Rojas, 2013**)**. Accordingly, we test this hypothesis further computing the mass balance analysis presented in Fig. 9 and performed south of Nelson Strait. Results suggest that the BC, flowing along the northern shelf of the SSI, may find Nelson Strait as a gateway for recirculation, thus supplying recurrently with source waters the BC flowing along the southern shelf of the SSI. We find this phenomenon is particularly noticeable during summer and winter, when the flux coming from the Nelson Strait appears to be feeding the BC more prominently (Fig. 9).

The decrease of the northeastward volume transport occurring east of King George Island, near transect T21, is attributed here to the start of the recirculation of the BC around the archipelago. We observe this pattern from spring to autumn, which agrees well with summertime geostrophic volume transport estimates presented in Sangrà et al. (2011), thus supporting the likely recurrence of this spatial feature through all seasons.

The year-round nature of the BC, as uncovered in this work, is especially relevant in that it shows the BC flows permanently at relatively the same strength, at least downstream of Nelson Strait, over a pathway of about 100 km. This opens a challenging question about the driving forces behind this recurrence through all seasons. The question here is whether the density gradient set by the water mass contrast between TBW and TWW also exists as a major driving force from autumn to spring. In this regard we highlight that future observational efforts must focus on assessing the seasonal hydrography of the BC with year-round mesoscale-solving measurements so that the year-round driving forces of the current might be better elucidated.

In Table 1 we summarize the present knowledge about velocity and volume transport estimates reported in the literature about the Bransfield Current. As previously introduced, most of these studies are based on summertime measurements and so the year-round description through seasons is presently lacking. These velocity values and volume transports are derived either from direct velocity measurements or from

Table 1
Summary of velocity observations and volume transport estimates of the Bransfield Current. The acronyms are: ADCP (Acoustic Doppler Current Profiler), CTD (Conductivity, Temperature and Depth), LADCP (Lowered Acoustic Doppler Current Profiler), SADCP (Shipboard Acoustic Doppler Current Profiler).

Reference	Velocity (cm s^{-1}) or Transport (Sv)	Instrument	Methodology for vel. or transp. estimate	Region	Date (month/year)
Grelowski et al., 1986	0.96 Sv	CTD	Geostrophic vel. relative to 500 db	South off Livingston I.	12/1983 – 01/1984
	1.09 Sv			South off Robert I.	(Spring – Summer)
	0.74 Sv			South off King George I.	
Niller et al., 1991	0.3 Sv / 8 cm s^{-1}	CTD	Geostrophic vel. relative to 200 db	Western Deception I.	11/1986 – 03/1987 (Spring – Summer)
López et al., 1999	1 Sv	CTD	Geostrophic vel. relative to 500 db	South off King George I.	01 – 02/1994 (Summer)
Gomis et al., 2002	0.5 Sv	CTD	Geostrophic vel. relative to 500 db	South off Livingston I.	12/1995 – 01/1996 (Spring – Summer)
Zhou et al., 2002	40 cm s^{-1}	Drifters at 15 and 40 *m*	Direct vel. observations	Along the southern SSI slope	11/1988 – 01/1990 (All seasons)
Zhou et al., 2006	40 – 50 cm s^{-1}	ADCP	Direct vel. observations	South off King George I.	03/2004 (Summer)
Morozov, 2007	0.8 Sv	LADCP	Direct vel. observations	South off Greenwich I.	11/2005(Spring)
Savidge and Amft, 2009	30 cm s^{-1}	SADCP	Geostrophic vel. relative to 500 db	South off Livingston I.	1997 – 2003 (Summer)
	40 cm s^{-1}			South off King George I.	
Sangrà et al., 2011	0.50 Sv	CTD	Geostrophic vel. relative to 500 db	South off Livingston I.	12/1999 (Spring) + 12/2002 – 01/2003 (Spring – Summer)
	0.73 Sv			South off Robert I.	
	0.88 Sv			South off King George I.	
Poulin et al., 2014	30 – 40 cm s^{-1}	ADCP	Direct vel. observations	South off the Nelson Strait	01/2010 (Summer)
Sangrà et al., 2017	0.31 – 0.49 Sv	CTD	Geostrophic vel. relative to 500 db	South off the Nelson Strait	01/2010 (Summer)
This study	0.93 Sv	SADCP	Direct vel. observations	Upstream of Nelson Strait (south off Livingston I. – Robert I.)	1999 – 2014 (Clim. summer
	0.88 Sv				Clim. autumn
	0.50 Sv			Downstream of Nelson Strait (south off Nelson I. – King George I.)	Clim. winter
	0.65 Sv				Clim. spring
	1.53 Sv				Clim. summer
	1.29 Sv				Clim. autumn
	1.20 Sv				Clim. winter
	1.22 Sv				Clim. spring)

hydrographic data (geostrophic velocities), then generally relative to 500 db. For each case in Table 1, we detail the origin of the values being provided.

Overall, volume transport estimates from previous works fall on the main within the same order of magnitude as results presented in this study, noting that existing discrepancies may be caused due to a comparison where different methodologies apply, and where synoptic measurements are compared against climatological values. To the best of our knowledge, this work delivers an unprecedented view of the spatio-temporal variability of the Bransfield Current transport along its full pathway south off the South Shetland Islands. Existing data gaps, especially in the upstream region of the current near Livingston Island during winter, and the data limitations that an irregular sampling implies, suggest that future observational and modeling efforts would

benefit a further understanding of the ocean dynamics in this region, thus assisting the study of the forcing mechanism behind the BC.

5. Conclusions

The Bransfield Current has been traditionally described as a summertime coastal jet flowing northeastward and hugging the South Shetland Islands slope while contouring the bathymetry of the archipelago and constrained by the Coriolis force (Niller et al., 1991; Zhou et al., 2002, 2006; García et al., 1994; Sangrà et al., 2011, 2017). Based on *in situ* hydrographic observations and laboratory experiments, previous authors have shown that the summertime circulation of the Bransfield Current agrees well with that of a buoyancy-driven coastal current (Sangrà et al., 2011, 2017; Poulin et al., 2014). The buoyancy-induced pressure gradient occurs between the relatively warmer and fresher TBW, leaning over the islands' slope, and the colder and saltier TWW, originated in the Weddell Sea and flooding into Bransfield Strait.

In this work we present an updated view of the seasonal circulation and volume transport driven by the Bransfield Current, following the pioneering work by Savidge and Amft (2009), where a summer-winter view follows from direct velocity measurements (SADCP data) collected between 1999 and 2003. To do this, we use a longer period of direct velocity observations (1999–2014), which also improve the spatial coverage in time. This novel approach and data extension allow us to characterize the velocity field and volume transport driven by the BC through all seasons and over nearly its entire pathway of circulation south of the SSI in an unprecedented manner.

This study confirms the BC is a year-round feature of the circulation in Bransfield Strait, flowing persistently towards the northeast along the southern slope of the SSI, a path of 170 km. We also find the recirculation around the archipelago, as described in previous summertime studies (Sangrà et al., 2011, 2017), is likely to occur also through other seasons, at least during winter and spring. These features are observed in the horizontal and vertical distributions of the velocity field in Figs. 4, 5 and 7.

Through the water column, the structure of the BC agrees well with the summertime and springtime views reported in previous works (Morozov, 2007; Savidge and Amft, 2009; Poulin et al., 2014), and describes the BC as a surface-intensified coastal jet whose velocities decrease at depth, particularly from 100-150 m towards deeper levels (Fig. 7). Also, we find the BC displays a coherent pattern depending on whether it finds to its left-hand side the islands' slope or a channel between islands (Fig. 7). Along the former case, the core of the BC leans on the island slope, while in the latter case, the core flows as a wedge-shaped current, missing an immediate boundary to its left-hand side.

Generally, the spatial variability of the BC displays two distinct regions: upstream and downstream of Nelson Strait. Upstream of Nelson Strait, the BC flows with an approximate core width of 20–30 km, which is slightly larger than the internal Rossby deformation radius for this region, $R_d = 10$ km (Grelowski et al., 1986; Chelton et al., 1998). This occurs from Livingston Island to Robert Island (transects T3-T9; Figs. 4 and 5), at least from spring to autumn. Winter data scarcity prevents us from an analogous statement during this season. Downstream of Nelson Strait, and towards King George Island (T11-T20), we find the BC widens through all seasons up to a width of about 40 km, much wider than the deformation radius (Figs. 4, 5 and 7). This widening is consistent with laboratory experiments reproducing the dynamics of the BC as a density-driven coastal current, hugging the simulated islands (a wall) to its left-hand side in a rotating tank (Sangrà et al., 2017). We argue that in the real ocean, the widening of the King George Island shelf might promote further the widening of the BC since, flowing from the surface down to at least 250 m depth, the jet will have to accommodate its width to contour the island slope further offshore.

The above description, in terms of the observed seasonal and spatial variability, suggests that Nelson Strait marks the transition between two different regions: upstream (T3-T9) and downstream (T11-T20) of Nelson Strait. Upstream of the Nelson Strait, the BC presents similar volume transports in summer, autumn and springtime (0.94 ± 0.15 Sv, 0.88 ± 0.19 Sv and 0.65 ± 0.13 Sv, respectively). During winter, the transport appears to decrease notably, as compared to other seasons, at least south off Greenwich Island (0.50 ± 0.04 Sv in transects T7-T9). Downstream of Nelson Strait, the seasonally-averaged estimates of volume transport suggest that no significant variability exists among seasons: 1.53 ± 0.17 Sv in summer, 1.29 ± 0.26 Sv in autumn, 1.20 ± 0.15 Sv in winter and 1.22 ± 0.20 Sv in spring.

The observed increase in volume transport after passing the Nelson Strait is consistent with prior summertime data presented in Savidge and Amft (2009) and Sangrà et al. (2011), based on direct velocity measurements and geostrophic velocity estimates, respectively. Our observations show this spatial pattern is also present through autumn, winter and spring based on direct velocity measurements. According to this finding, we also performed a mass balance analysis which suggests the downstream increase of the BC volume transport is likely due to a recurrent inflow of source waters coming seasonally from the northern slope of the SSI and passing through the Nelson Strait (Fig. 9).

Overall, results from this work highlight that future modeling and observational efforts must be addressed to cover existing gaps about the dynamics of the BC, especially in the upstream region of the current near Livingston Island during winter. In this line, the seasonal hydrography of the Bransfield Current must also be investigated further based on mesoscale-solving measurements close to the islands' coastlines, especially when noting that the Bransfield Current has been shown in the past to propagate as a summertime buoyancy-driven coastal jet transporting relatively warm and fresh Transitional Zonal Water with Bellingshausen influence (Sangrà et al., 2011, 2017), whose presence in Bransfield Strait might be limited during seasons different from summer.

We conclude this work delivers an unprecedented view of the spatio-temporal variability of the Bransfield Current seasonal circulation and volume transport along its full pathway south off the South Shetland Islands, where our results agree well with independent estimates and descriptions from previous works (Table 1).

Declaration of Competing Interest

The authors declare that they have no known competing financial interests or personal relationships that could have appeared to influence the work reported in this paper.

Acknowledgements

This work has been supported by the Spanish government (Ministerio de Economía y Competitividad) through the projects FLUXES (CTM2015-69392-C3-3-R), SAGA (RTI2018-100844-B-C31) and e-IMPACT (PID2019-109084RB-C21). The first author is also grateful to the Canary government (Consejería de Economía, Conocimiento y Empleo, Agencia Canaria de Investigación, Innovación y Sociedad de la Información) for the financial support awarded through a PhD scholarship (TESIS2021010025). Finally, the authors wish to thank two anonymous reviewers for their thoughtful comments to improve this paper.

References

Chelton, D.B., DeSzoeke, R.A., Schlax, M.G., El Naggar, K., Siwertz, N., 1998. Geographical variability of the first baroclinic Rossby radius of deformation. J. Phys. Oceanogr. 28 (3), 433–460.

Cook, A.J., Holland, P.R., Meredith, M.P., Murray, T., Luckman, A., Vaughan, D.G., 2016. Ocean forcing of glacier retreat in the western Antarctic Peninsula. Science 353 (6296), 283–286.

Dotto, T.S., Mata, M., Kerr, R., Garcia, C., 2021. A novel hydrographic gridded data set for the northern Antarctic Peninsula. Earth Syst. Sci. Data 13, 671–696.

Firing, Eric, Hummon, Julia, Chereskin, Teresa, 2012. Improving the quality and accessibility of current profile measurements in the Southern Ocean. Oceanography 25 (3), 164–165.

Fischer, J., Visbeck, M., 1993. Deep velocity profiling with self-contained ADCPs. J. Atmos. Oceanic Technol. 10 (5), 764–773.
García, M.A., López, O., Sospedra, J., Espino, M., Gràcia, V., Morrison, G., Rojas, P., Figa, J., Puigdefàbregas, J., Arcilla, A.S., 1994. Mesoscale variability in the Bransfield Strait region (Antarctica) during Austral summer. Ann. Geophys. 12 (9), 856–867.
García, M.A., Castro, C.G., Ríos, A.F., Doval, M.D., Rosón, G., Gomis, D., López, O., 2002. Water masses and distribution of physico-chemical properties in the Western Bransfield Strait and Gerlache Strait during Austral summer 1995/96. Deep Sea Res. Part II 49 (4–5), 585–602.
García-Muñoz, C., Sobrino, C., Lubián, L.M., García, C.M., Martínez-García, S., Sangrà, P., 2014. Factors controlling phytoplankton physiological state around the South Shetland Islands (Antarctica). Mar. Ecol. Prog. Ser. 498, 55–71.
Gomis, Damià, García, Marc A., López, Oswaldo, Pascual, Ananda, 2002. Quasi-geostrophic 3D circulation and mass transport in the western Bransfield Strait during Austral summer 1995/96. Deep Sea Res. Part II 49 (4-5), 603–621.
Gordo Rojas, M. C. (2013). *Sistema de la Corriente del Bransfield, SCB (Antártida)* (Doctoral dissertation).
Grelowski, A., Majewicz, A., Pastuszak, M., 1986. Mesoscale hydrodynamic processes in the region of Bransfield Strait and the southern part of Drake Passage during BIOMASS-SIBEX 1983–1984. Polish Polar Research 7 (4).
Hofmann, E.E., Klinck, J.M., Lascara, C.M., Smith, D.A., 1996. Water mass distribution and circulation west of the Antarctic Peninsula and including Bransfield Strait. Foundations for ecological research west of the Antarctic Peninsula 70, 61–80.
Instruments, T.R., 2013. TRDI ADCP Datasheet, Ocean. Surveyor.
John D'Errico (2022). inpaint_nans (https://www.mathworks.com/matlabcentral/fileexchange/4551-inpaint_nans), MATLAB Central File Exchange. Retrieved February 10, 2022.
Kreczmer, K., Dąbski, M., Zmarz, A., 2021. Terrestrial Signature of a recently-tidewater glacier and adjacent periglaciation, Windy Glacier (South Shetland Islands, Antarctic). Front. Earth Sci. 9, 299.
Lenn, Y.D., Chereskin, T.K., Sprintall, J., Firing, E., 2007. Mean jets, mesoscale variability and eddy momentum fluxes in the surface layer of the Antarctic Circumpolar Current in Drake Passage. J. Mar. Res. 65 (1), 27–58.
López, O., García, M.A., Gomis, D., Rojas, P., Sospedra, J., Sánchez-Arcilla, A., 1999. Hydrographic and hydrodynamic characteristics of the eastern basin of the Bransfield Strait (Antarctica). Deep Sea Res. Part I 46 (10), 1755–1778.
Morozov, E.G., 2007. Currents in Bransfield Strait. Dokl. Earth Sc. 415 (2), 984–986.
Münchow, A., Garvine, R.W., 1993. Dynamical properties of a buoyancy-driven coastal current. J. Geophys. Res. Oceans 98 (C11), 20063–20077.
Niller, P.P., Amos, A., Hu, J.H., 1991. Water masses and 200 m relative geostrophic circulation in the western Bransfield Strait region. Deep Sea Res. Part A 38 (8–9), 943–959.
Padman, L., Fricker, H.A., Coleman, R., Howard, S., Erofeeva, L., 2002. A new tide model for the Antarctic ice shelves and seas. Ann. Glaciol. 34, 247–254.
Poulin, F.J., Stegner, A., Hernández-Arencibia, M., Marrero-Díaz, A., Sangrà, P., 2014. Steep shelf stabilization of the coastal Bransfield Current: Linear stability analysis. J. Phys. Oceanogr. 44 (2), 714–732.
Sangrà, P., Gordo, C., Hernández-Arencibia, M., Marrero-Díaz, A., Rodríguez-Santana, A., Stegner, A., Martínez-Marrero, A., Pelegrí, J., Pichon, T., 2011. The Bransfield current system. Deep Sea Res. Part I 58 (4), 390–402.
Sangrà, P., Stegner, A., Hernández-Arencibia, M., Marrero-Díaz, Á., Salinas, C., Aguiar-González, B., Henríquez-Pastene, C., Mouriño-Carballido, B., 2017. The Bransfield gravity current. Deep Sea Res. Part I 119, 1–15.
Savidge, D.K., Amft, J.A., 2009. Circulation on the West Antarctic Peninsula derived from 6 years of shipboard ADCP transects. Deep Sea Res. Part I 56 (10), 1633–1655.
Teira, E., Mourino-Carballido, B., Martinez-Garcia, S., Sobrino, C., Ameneiro, J., Hernandez-Leon, S., Vazquez, E., 2012. Primary production and bacterial carbon metabolism around South Shetland Islands in the Southern Ocean. Deep Sea Res. Part I 69, 70–81.
Tokarczyk, R., 1987. Classification of water masses in the Bransfield Strait and southern part of the Drake Passage using a method of statistical multidimensional analysis. Polish Polar Research 4 (08).
Zhang, Y., Seidel, D.J., Golaz, J.C., Deser, C., Tomas, R.A., 2011. Climatological characteristics of Arctic and Antarctic surface-based inversions. J. Clim. 24 (19), 5167–5186.
Zhou, M., Niller, P.P., Hu, J.H., 2002. Surface currents in the Bransfield and Gerlache straits, Antarctica. Deep Sea Res. Part I 49 (2), 267–280.
Zhou, M., Niller, P.P., Zhu, Y., Dorland, R.D., 2006. The western boundary current in the Bransfield Strait, Antarctica. Deep Sea Res. Part I 53 (7), 1244–1252.